Research Article Vol. 26, No. 6 | 19 Mar 2018 | OPTICS EXPRESS 7022

Optics EXPRESS

Directly modulated 1.3 μm quantum dot lasers epitaxially grown on silicon

DAISUKE INOUE,[1,2,5,*] DAEHWAN JUNG,[2,5] JUSTIN NORMAN,[3] YATING WAN,[4] NOBUHIKO NISHIYAMA,[1] SHIGEHISA ARAI,[1] ARTHUR C. GOSSARD,[2,3,4] AND JOHN E. BOWERS,[2,3,4]

[1] *Institute of Innovative Research, Tokyo Institute of Technology, Tokyo 152-8552, Japan*
[2] *Institute for Energy Efficiency, University of California Santa Barbara, Santa Barbara, California 93106, USA*
[3] *Department of Electrical and Computer Engineering, University of California Santa Barbara, Santa Barbara, California 93106, USA*
[4] *Materials Department, University of California Santa Barbara, Santa Barbara, California 93106, USA*
[5] *These authors contributed equally to this work*
[*] *inoue.d.ac@gmail.com*

Abstract: We report the first demonstration of direct modulation of InAs/GaAs quantum dot (QD) lasers grown on on-axis (001) Si substrate. A low threading dislocation density GaAs buffer layer enables us to grow a high quality 5-layered QD active region on on-axis Si substrate. The active layer has *p*-modulation doped GaAs barrier layers with a hole concentration of 5×10^{17} cm^{-3} to suppress gain saturation. Small-signal measurement on a 3 × 580 μm^2 Fabry-Perot laser showed a 3dB bandwidth of 6.5 GHz at a bias current of 116 mA. A 12.5 Gbit/s non-return-to-zero signal modulation was achieved by directly probing the chip. Open eyes with an extinction ration of 3.3dB was observed at room temperature. The bit-error-rate (BER) curve showed no error-floor up to BER of 1×10^{-13}. 12 km single-mode fiber transmission experiments using the QD laser on Si showed a low power penalty of 1 dB at 5 Gbit/s. These results demonstrate the potential for QD lasers epitaxially grown on Si to be used as a low-cost light source for optical communication systems.

OCIS codes: (250.5960) Semiconductor lasers; (230.5590) Quantum-well, -wire and -dot devices; (060.4080) Modulation.

References and links

1. A. Vahdat, H. Liu, X. Zhao, and C. Johnson, "The emerging optical data center," in Optical Fiber Communication Conference (OFC), 2011 OSA Technical Digest Series (Optical Society of America, 2011),paper OTuH2.
2. J. A. Tatum, D. Gazula, L. A. Graham, J. K. Guenter, R. H. Johnson, J. King, C. Kocot, G. D. Landry, I. Lyubomirsky, A. N. MacInnes, E. M. Shaw, K. Balemarthy, R. Shubochkin, D. Vaidya, M. Yan, and F. Tang, "VCSEL-based interconnects for current and future data centers," J. Lightwave Technol. **33**(4), 727–732 (2015).
3. T. Tadokoro, W. Kobayashi, T. Fujisawa, T. Yamanaka, and F. Kano, "High-speed modulation lasers for 100GbE applications," in Optical Fiber Communication Conference/National Fiber Optic Engineers Conference, OSA Technical Digest Series (Optical Society of America, 2011), paper OWD1.
4. K. Otsubo, N. Hatori, M. Ishida, S. Okumura, T. Akiyama, Y. Nakata, H. Ebe, M. Sugawara, and Y. Arakawa, "Temperature-insensitive eye-opening under 10-Gb/s modulation of 1.3-µm p-doped quantum-dot lasers without current adjustments," Jpn. J. Appl. Phys. **43**(8B), L1124–L1126 (2004).
5. M. Ishida, M. Matsuda, Y. Tanaka, K. Takada, M. Ekawa, T. Yamamoto, T. Kageyama, M. Yamaguchi, K. Nishi, M. Sugawara, and Y. Arakawa, "Temperature-stable 25-Gbps direct-modulation in 1.3-µm InAs/GaAs quantum dot lasers," in Lasers and Electro-Optics (CLEO) Conference, 2012 OSA Technical Digest Series (Optical Society of America, 2012), paper CM1I.2.
6. S. Banyoudeh, O. Eyal, A. Abdollahinia, F. Schnabel, V. Sichkovskyi, J. P. Reithmaier, and G. Eisenstein, "High-bandwidth temperature-stable 1.55-µm quantum dot lasers," Proc. SPIE **10123**, 1012306 (2017).
7. P. De Dobbelaere, S. Abdalla, S. Gloeckner, M. Mack, G. Masini, A. Mekis, T. Pinguet, S. Sahni, A. Narasimha, D. Guckenberger, and M. Harrison, "Si photonics based high-speed optical transceivers," in European Conference and Exhibition on Optical Communication, OSA Technical Digest Series (Optical Society of America, 2012), paper We.1.E.5.

#321372 https://doi.org/10.1364/OE.26.007022
Journal © 2018 Received 6 Feb 2018; revised 25 Feb 2018; accepted 25 Feb 2018; published 7 Mar 2018

Corrected: 3 April 2018

8. T. Komljenovic, M. Davenport, J. Hulme, A. Y. Liu, C. T. Santis, A. Spott, S. Srinivasan, E. J. Stanton, C. Zhang, and J. E. Bowers, "Heterogeneous silicon photonic integrated circuits," J. Lightwave Technol. **34**(1), 20–35 (2016).
9. S. Tanaka, S. H. Jeong, S. Sekiguchi, T. Kurahashi, Y. Tanaka, and K. Morito, "High-output-power, single-wavelength silicon hybrid laser using precise flip-chip bonding technology," Opt. Express **20**(27), 28057–28069 (2012).
10. G. Kurczveil, D. Liang, M. Fiorentino, and R. G. Beausoleil, "Robust hybrid quantum dot laser for integrated silicon photonics," Opt. Express **24**(14), 16167–16174 (2016).
11. T. Kita, N. Yamamoto, T. Kawanishi, and H. Yamada, "Ultra-compact wavelength-tunable quantum-dot laser with silicon-photonics double ring filter," Appl. Phys. Express **8**(6), 062701 (2015).
12. T. Morishita, K. Kounoike, S. Fujiwara, Y. Hagi, and Y. Yabuhara, "Crystal growth and wafer processing of indium phosphide 6" substrate,"in Proc. of the 2016 International Conference on Compound Semiconductor Manufacturing Technology(MANTECH' 2016), Florida, United States (2016), paper 5b.1.
13. A. Y. Liu, S. Srinivasan, J. Norman, A. C. Gossard, and J. E. Bowers, "Quantum dot lasers for silicon photonics," Photon. Res. **3**(5), B1–B9 (2015).
14. H. Kroemer, T.-Y. Liu, and P. M. Petroff, "GaAs on Si and related systems: Problems and prospects," J. Cryst. Growth **95**(1–4), 96–102 (1989).
15. A. Y. Liu, C. Zhang, J. Norman, A. Snyder, D. Lubyshev, J. M. Fastenau, A. W. Liu, A. C. Gossard, and J. E. Bowers, "High performance continuous wave 1.3 μm quantum dot lasers on silicon," Appl. Phys. Lett. **104**(4), 041104 (2014).
16. S. Chen, W. Li, J. Wu, Q. Jiang, M. Tang, S. Shutts, S. Elliott, A. Sobiesierski, A. Seeds, I. Ross, P. Smowton, and H. Liu, "Electrically pumped continuous-wave III–V quantum dot lasers on silicon," Nat. Photonics **10**(5), 307–311 (2016).
17. J. Norman, M. J. Kennedy, J. Selvidge, Q. Li, Y. Wan, A. Y. Liu, P. G. Callahan, M. P. Echlin, T. M. Pollock, K. M. Lau, A. C. Gossard, and J. E. Bowers, "Electrically pumped continuous wave quantum dot lasers epitaxially grown on patterned, on-axis (001) Si," Opt. Express **25**(4), 3927–3934 (2017).
18. Y. Wan, J. Norman, Q. Li, M. J. Kennedy, D. Liang, C. Zhang, D. Huang, Z. Zhang, A. Y. Liu, A. Torres, D. Jung, A. C. Gossard, E. L. Hu, K. M. Lau, and J. E. Bowers, "1.3 μm submilliamp threshold quantum dot micro-lasers on Si," Optica **4**(8), 940–944 (2017).
19. A. Y. Liu, J. Peters, X. Huang, D. Jung, J. Norman, M. L. Lee, A. C. Gossard, and J. E. Bowers, "Electrically pumped continuous-wave 1.3 μm quantum-dot lasers epitaxially grown on on-axis (001) GaP/Si," Opt. Lett. **42**(2), 338–341 (2017).
20. D. Jung, J. Norman, M. J. Kennedy, C. Shang, B. Shin, Y. Wan, A. C. Gossard, and J. E. Bowers, "High efficiency low threshold current 1.3 μm InAs quantum dot lasers on on-axis (001) GaP/Si," Appl. Phys. Lett. **111**(12), 122107 (2017).
21. Y.-H. Jhang, R. Mochida, K. Tanabe, K. Takemasa, M. Sugawara, S. Iwamoto, and Y. Arakawa, "Direct modulation of 1.3 μm quantum dot lasers on silicon at 60 °C," Opt. Express **24**(16), 18428–18435 (2016).
22. D. Jung, Z. Zhang, J. Norman, R. Herrick, M. J. Kennedy, P. Patel, K. Turnlund, C. Jan, Y. Wan, A. C. Gossard, and J. E. Bowers, "Highly reliable low threshold InAs quantum dot lasers on on-axis (001) Si with 87% injection efficiency," ACS Photonics (to be published).
23. D. Jung, P. G. Callahan, B. Shin, K. Mukherjee, A. C. Gossard, and J. E. Bowers, "Low threading dislocation density GaAs growth on on-axis GaP/Si (001)," J. Appl. Phys. **122**(22), 225703 (2017).
24. R. L. Nagarajan, M. Ishikawa, T. Fukushima, R. S. Geels, and J. E. Bowers, "High speed quantum well lasers and carrier transport effects," IEEE J. Quantum Electron. **28**(10), 1990–2008 (1992).
25. W. Kobayashi, T. Ito, T. Yamanaka, T. Fujisawa, Y. Shibata, T. Kurosaki, M. Kohtoku, T. Tadokoro, and H. Sanjoh, "50-Gb/s direct modulation of 1.3-µm InGaAlAs-based DFB laser with ridge waveguide structure," IEEE J. Sel. Top. Quantum Electron. **19**(4), 1500908 (2013).
26. Y. Matsui, T. Pham, T. Sudo, G. Carey, B. Young, J. Xu, C. Cole, and C. Roxlo, "28-Gbaud PAM4 and 56-Gb/s NRZ performance comparison using 1310-nm Al-BH DFB Laser," J. Lightwave Technol. **34**(11), 2677–2683 (2016).
27. K. T. Tan, C. Marinelli, M. G. Thompson, A. Wonfor, M. Silver, R. L. Sellin, R. V. Penty, I. H. White, M. Kuntz, M. Lammlin, N. N. Ledentsov, D. Bimberg, A. E. Zhukov, V. M. Ustinov, and A. R. Kovsh, "High bit rate and elevated temperature data transmission using InGaAs quantum-dot lasers," IEEE Photonics Technol. Lett. **16**(5), 1415–1417 (2004).
28. B. Dagens, A. Martinez, J. G. Provost, D. Make, Q. Le Gouezigou, L. Ferlazzo, K. Merghem, A. Lemaître, A. Ramdane, and B. Thedrez, "High extinction ratio and high-temperature 2.5-Gb/s floor-free 1.3-µm transmission with a directly modulated quantum dot laser," IEEE Photonics Technol. Lett. **18**(4), 589–591 (2006).
29. M. Ishida, Y. Tanaka, K. Takada, T. Yamamoto, H. Z. Song, Y. Nakata, M. Yamaguchi, K. Nishi, M. Sugawara, and Y. Arakawa, "Effect of carrier transport on modulation bandwidth of 1.3-µm InAs/GaAs self-assembled quantum-dot lasers," in Proc. of the22nd IEEE International Semiconductor Laser Conference2012 (ISLC 2012), Kyoto, Japan (2012), paper WD4.
30. T. Kageyama, K. Watanabe, Q. H. Vo, K. Takemasa, M. Sugawara, S. Iwamoto, and Y. Arakawa, "InAs/GaAs quantum dot lasers with GaP strain-compensation layers grown by molecular beam epitaxy," Phys. Status Solidi., A Appl. Mater. Sci. **213**(4), 958–964 (2016).

31. T. Kageyama, Q. H. Vo, K. Watanabe, K. Takemasa, M. Sugawara, S. Iwamoto, and Y. Arakawa,“Large modulation bandwidth (13.1 GHz) of 1.3 μm-range quantum dot lasers with high dot density and thin barrier layer,” in Proceedings of the Compound Semiconductor Week 2016 (CSW’2016), Toyama, Japan(2016), paper MoC3–4.
32. D. Arsenijević and D. Bimberg, “Quantum-dot lasers for 35 Gbit/s pulse-amplitude modulation and 160 Gbit/s differential quadrature phase-shift keying,” Proc. SPIE **9892**, 98920S (2016).
33. J. E. Bowers, B. R. Hemenway, A. H. Gnauck, and D. P. Wilt, “High-speed InGaAsP constricted-mesa lasers,” IEEE J. Quantum Electron. **22**(6), 833–844 (1986).
34. C. Henry, “Theory of the linewidth of semiconductor lasers,” IEEE J. Quantum Electron. **18**(2), 259–264 (1982).
35. T. L. Koch and J. E. Bowers, “Nature of wavelength chirping in directly modulated semiconductor lasers,” Electron. Lett. **20**(25–26), 1038–1040 (1984).

1. Introduction

The need for high capacity optical links has rapidly increased due to the rapid growth of data centers and the Internet [1]. In the past decade, a low cost and energy efficient light source has been developed and implemented in optical transceivers. Vertical-cavity surface-emitting lasers (VCSELs) are adopted as a directly modulated light source, since the low-threshold and high bandwidth enable energy efficient operation [2]. Distributed-feedback (DFB) lasers are also used as both light source for external modulator and directly modulated laser [3]. In advanced optical link applications, quantum dot (QD) based optical devices instead of quantum well (QW) are expected to perform better for many applications such as mode-locked lasers, multiple wavelength lasers and temperature insensitive light sources. Therefore, QD lasers are of great interest for direct modulation in uncooled environment. For instance, 10.3 Gbit/s operation of InAs/GaAs QD laser for wide temperature range from –40°C to 80°C has been reported [4]. Temperature stable 25 Gbit/s operations have been demonstrated for both 1.3 μm InAs/GaAs QD laser [5] and 1.55 μm InAs/InP QD laser [6].

For low-cost optical components, the use of III-V lasers with silicon photonics circuits that can be manufactured by complementary metal-oxide-semiconductor (CMOS) compatible processes is an attractive approach [7]. To integrate III/V lasers to silicon photonics, heterogeneous wafer bonding [8] or flip-chip mounting [9] are utilized. There are reports for QD active layer integrated with silicon photonics circuits using wafer bonding [10] and chip-mounting [11]. A multiple die to wafer bonding can overcome the difference of maximum available wafer size between 150 mm for III/V (GaAs, InP) [12] and 450 mm for Si. However, this method increases the complexity of fabrication process and manufacturing cost. Therefore, wafer-scale monolithic integration and processing is interesting for mitigating the complexity of bonding as well as alignment cost [13].

Growth of III-V materials on Si results in a high density of threading-dislocations (TDs) and antiphase domains (APDs) due to the large lattice mismatch and polar/non-polar heterointerface, respectively [14]. Epitaxially grown QD lasers, however, have shown much higher defect-tolerance than QW lasers, thanks to effective lateral carrier confinement in individual dots [15,16]. To be fully compatible with CMOS foundry process, QD lasers have been recently migrated from 4 to 6 ° offcut Si to on-axis (001) Si via patterned Si [17,18] or GaP intermediate buffer layer on Si [19,20]. Even with the considerable improvements in the QD Si laser performance over the last few years, there have been no reports about direct modulation characteristics of QD lasers epitaxially grown on Si. Direct modulation of QD lasers on Si can only be found for bonded device which operated at 6 Gbit/s up to 60°C [21]. Recently, we have demonstrated low threshold (<10 mA), high temperature (85°C) operation of QD lasers on Si with high injection efficiency (87%) and long lifetimes (>10 million hours at 35°C), which enables measurements of various unresolved dynamic characteristics of the QD Si lasers [22].

In this paper, to the best of our knowledge, we report direct-modulation characteristics of 1.3 μm InAs QD laser grown on on-axis (001) substrate for the first time. The measured device has a cavity length of 580 μm and a ridge stripe width of 5μm. The 3dB bandwidth of 6.5 GHz was obtained from small-signal modulation. The obtained *K*-factor of 0.92 ns is comparable to that of QD lasers grown on GaAs substrate. The eye opening was confirmed up to data-rate of 12.5 Gbit/s. In a bit-error-rate (BER) measurement, no error-floor was observed down to BER of 1×10^{-13} at the data-rate of 12.5 Gbit/s. Also, fiber transmission experiments were performed over 12 km standard single-mode fiber.

2. Fabrication and device structure

QD lasers were grown by solid-source molecular beam epitaxy. Figure 1 shows a schematic of the full laser epitaxial structure. A low threading dislocation density (~7×10^6 cm^{-2}) GaAs buffer layer was first grown on a GaP/Si wafer to improve the laser performance and reliability [23]. Then, five InAs QD layers sandwiched by a AlGaAs/GaAs graded-index separate-confinement-heterostructure were grown on the GaAs/Si template. To enhance the direct modulation efficiency, the GaAs barriers were *p*-modulation-doped (*p*-MD) at a nominal hole concentration of 5×10^{17} cm^{-3}. The QD density is 5×10^{10} cm^{-2}, and the acceptor per QD ratio is ~10. Specifically, the first 10 nm GaAs barrier after the QD layer was unintentionally doped (UID) while the following 10 nm GaAs layer was doped by Be. The subsequent 17.5 nm GaAs barrier was undoped to complete the GaAs barrier structure. For comparison, we also grew a nominally identical QD laser structure without the *p*-MD GaAs barrier. Other detailed growth conditions can be found elsewhere [20].

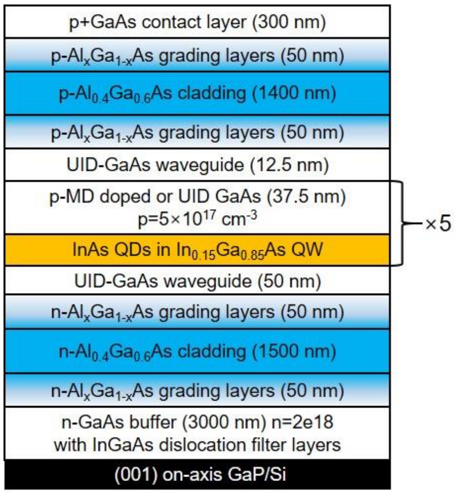

Fig. 1. A cross-sectional schematic of InAs QD laser epitaxial structure on Si.

The epi-materials were fabricated into narrow ridge-waveguide lasers via standard photolithography and dry-etching. Figure 2(a) shows a scanning electron microscope image of a processed laser. The laser ridge was deeply etched so that both *p* and *n* contact metals can be deposited on the epi-side. A 1-μm-thick SiO_2 was used as an isolation layer between the contact and probe metals. This two-top contact metal scheme enabled a low laser turn-on voltage by avoiding the GaAs/Si heterointerface, as will be shown in Fig. 3. The processed laser dies were thinned to ~150 μm for cleaving. The optical microscope image of Fig. 2(b) shows four QD lasers on a cleaved bar (900-μm-long lasers shown). Then, one of the facets was coated with 8 pairs of SiO_2/Ta_2O_5 films to achieve a low mirror loss (99% reflection). Figure 2(c) shows a schematic cross section of a QD laser on Si. It should be noted that the design of the electrodes has not yet been optimized for high-frequency operation.

Figure 3 displays light-current-voltage curves from a 5.0×580 μm^2 Fabry-Perot *p*-doped QD laser at RT (20 °C). Note the turn-on voltage of our epitaxially grown QD Si laser is only ~1 V, which is significantly lower than the QD lasers bonded onto Si (~4 V) [21]. The measured laser shows a CW threshold current of 14 mA and slope efficiency of 0.26 W/A. The maximum ground-state output power is more than 30 mW.

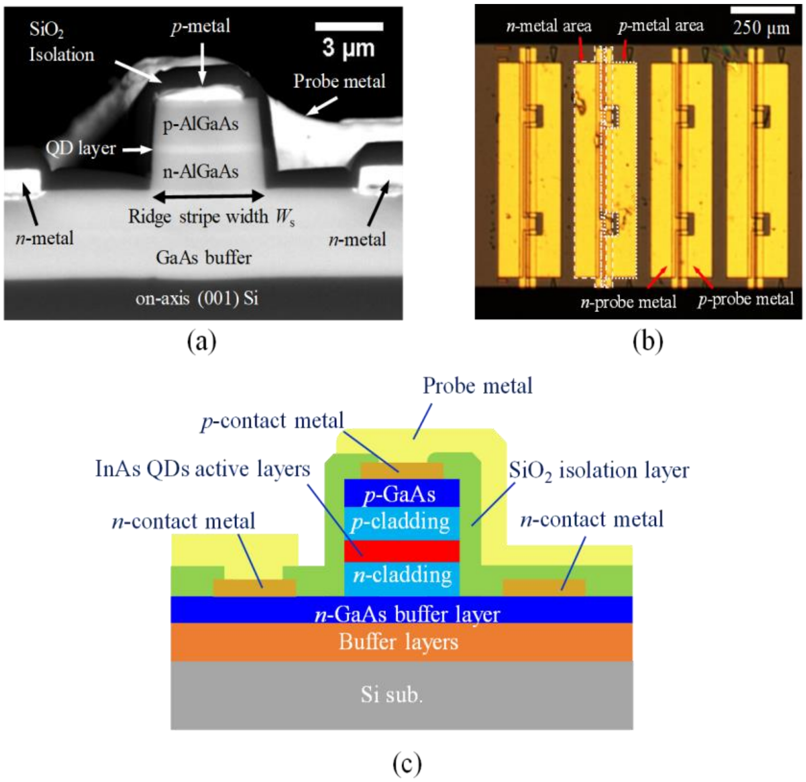

Fig. 2. (a) A cross-sectional scanning electron microscope image of a fabricated QD laser diode. (b) Optical microscope image to show four Fabry-Perot lasers from a cleaved laser bar. (c) Schematic cross-section of a ridge-waveguide QD laser on Si.

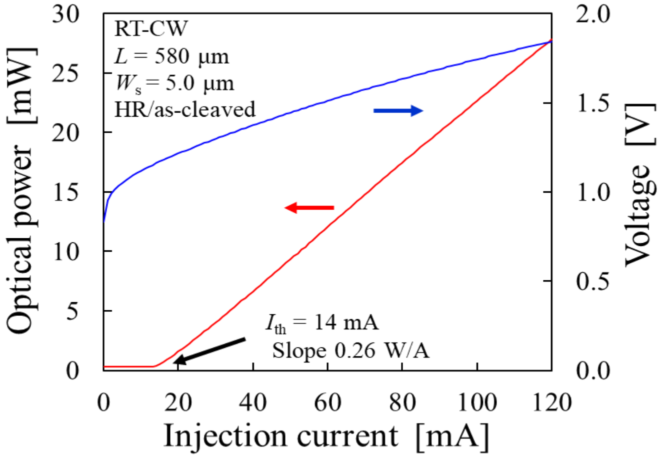

Fig. 3. Continuous wave light-current-voltage curves from a 5.0 × 580 μm^2 *p*-doped QD laser on Si at 20 °C.

3. Small-signal measurement

The small-signal response, S_{21}, was measured by directly probing the device using a signal/ground (SG) RF probe. A 20 GHz lightwave component analyzer (LCA, HP8703A) was used for the measurement. A QD laser chip was placed on a heat sink without any temperature control. Bias current to the QD laser was injected via the internal bias-tee of the LCA. The light output of the QD laser was collected by a spherical-lensed single-mode fiber and modulated light output was detected by an internal detector of the LCA. Figure 4 shows small-signal modulation responses S_{21} of the *p*-MD QD laser on Si at the bias currents of 20, 32, 52, 80 and 116 mA. These responses are normalized at low-frequency. To extract the damping rate γ and relaxation oscillation frequency f_r, a following three-pole fitting function H(*f*) [24] was used to draw fitting curves,

$$H(f) = \frac{1}{(1+(2\pi f\tau_p)^2)}\frac{f_r^4}{(f_r^2 - f^2)^2 + (\gamma f/2\pi)^2}, \qquad (1)$$

where τ_p stands for the RC or carrier transport delay. The fitting curves are also shown in Fig. 4 as gray colored solid lines. The 3dB bandwidth, f_{3dB} increased as the bias current was increased. The maximum f_{3dB} was 6.5 GHz at the bias current of 116 mA. The flat frequency response obtained at the high bias condition comes from strong damping characteristics of the QD active layer.

To verify the effect of *p*-doping in the barrier layers, small-signal responses of the identical structure device except for doping level of the barrier layers were compared. Figures 5(a) and (b) show small-signal responses for the devices with UID barriers and *p*-MD barriers. Both devices have a ridge stripe width of 3.0 μm, cavity length of 580 μm and HR coating at one side of the facets. Thus, these devices are expected to have same *RC* cutoff frequency. The UID device has a lower threshold current of 5.5 mA than that of *p*-doped device of 10mA. The frequency response of the UID device saturated at low bias current condition of 69.5 mA. In addition, the dip in the frequency response was observed at around 3 GHz. The maximum f_{3dB} was 4 GHz at the bias current of 69.5 mA. In contrast, the *p*-doped device showed flat response up to 3dB bandwidth. The bandwidth was increased until the bias current of 110 mA. The *p*-doping in the barriers provides built-in holes in the active region which suppress the hole depletion and help the carrier transport to the dot active layers.

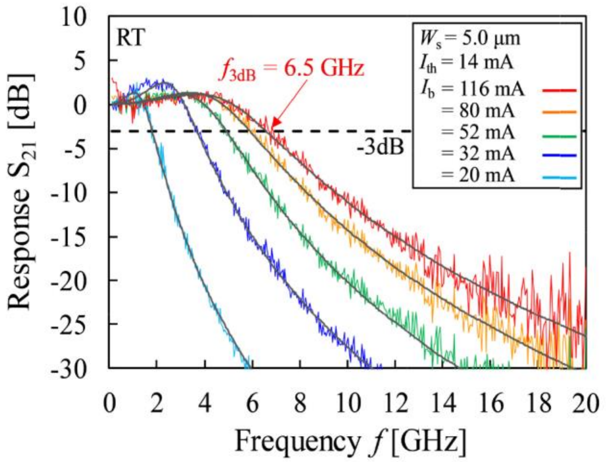

Fig. 4. Small-signal modulation responses for the QD laser on Si (5.0 × 580 μm^2) biased from 20 to 116 mA. The fitting curves are drawn using Eq. (1).

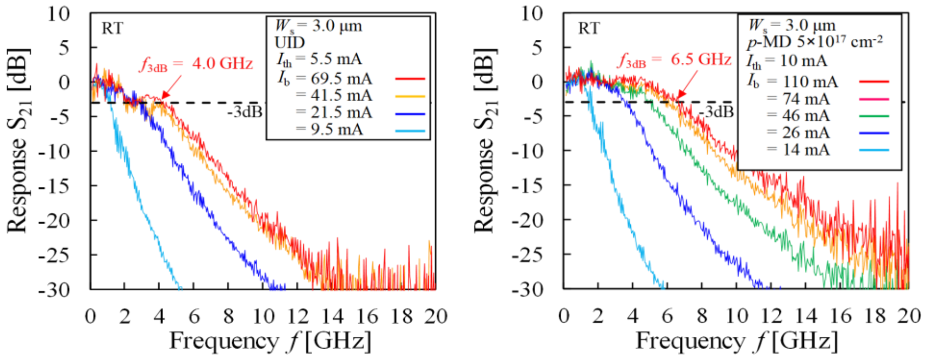

(a) (b)

Fig. 5. Comparison of small signal modulation response between (a) UID device and (b) *p*-MD device. These devices have identical device geometry except for doping in the barrier layers.

Figure 6 shows the plots of f_{3dB} and f_r of the *p*-doped QD laser shown in Fig. 4 as a function of square root of bias current above threshold obtained from fitting curves. The modulation efficiencies for f_{3dB} and f_r are 0.74 GHz/mA$^{1/2}$ and 0.68 GHz/mA$^{1/2}$. These slopes are calculated using plots below $(I_b - I_{th})^{1/2} < 7$ mA$^{1/2}$. These values are small compared with state-of-the-art QW lasers for direct modulation that have the modulation efficiency for f_r of 3–4 GHz/mA$^{1/2}$ [25,26]. This is due to the lower confinement factor and by gain compression caused by slow carrier capture in the QD active layer. The *K*-factor is derived by plotting the damping rate γ versus squared f_r. In Fig. 7, the linear fitting is drawn using the following equation,

$$\gamma = K \cdot f_r^2 + \gamma_0, \tag{2}$$

where γ_0 represents damping offset. The *K*-factor is estimated to be 0.92 ns from the slope of the fitting curve. The maximum 3 dB bandwidth limited by *K*-factor ($f_{3dB,\ max}$) can be calculated by the following equation,

$$f_{3dB,\max} = \frac{2\sqrt{2}\pi}{K}. \tag{3}$$

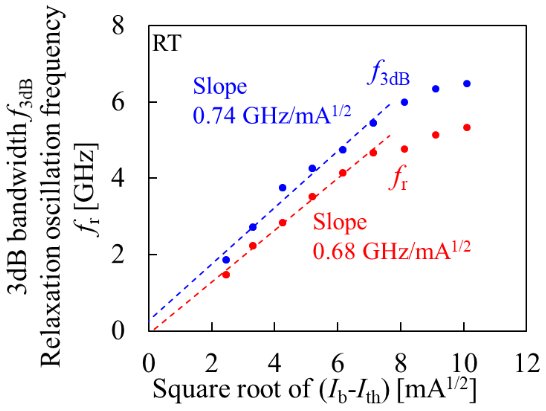

Fig. 6. 3dB bandwidth f_{3dB} and relaxation oscillation frequency f_r versus square-root of the bias current above threshold for the *p*-doped QD laser on Si (5.0 × 580 µm^2).

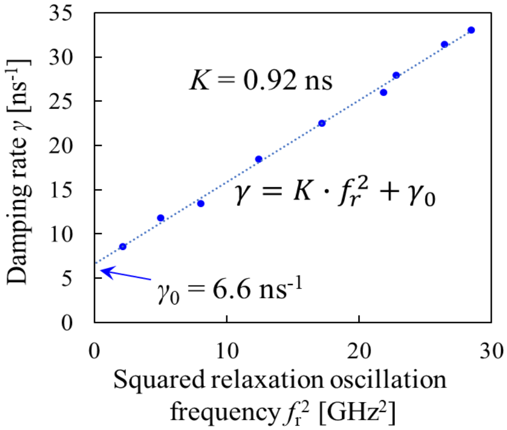

Fig. 7. Damping rate γ versus squared relaxation oscillation frequency f_r^2. The maximum 3 dB bandwidth limited by K-factor $f_{3dB,\ max}$ is 9.5 GHz.

The maximum $f_{3dB,\ max}$ is calculated to be 9.5 GHz. Hence, the measured f_{3dB} of 6.5 GHz from our small signal modulation is close to this K-factor limited bandwidth, but is lower due to a large pad capacitance of the electrodes, which are not optimized for high-frequency operation. Table 1 summarizes device parameters of this work and previously reported 1.3 µm InAs/GaAs QD lasers grown on GaAs substrate with ground-state lasing. There is a tendency that *p*-doped active layer shows better performance than the UID active layer in terms of *K*-factor. A record-high bandwidth among the 1.3 µm InAs/GaAs QD lasers has been reported to be 13.1 GHz in 2016 by Kageyama *et al.* [31] by reducing the GaAs barrier thickness. While the QD laser on Si has slightly inferior 3dB bandwidth and modulation efficiency, the obtained *K*-factor is comparable to that of the QD lasers on GaAs. To improve the modulation performance of QD lasers on Si, there is still room to increase the dot density to enhance differential gain. Moreover, a graded *p*-modulation doping could improve the carrier transport further [32].

Table 1. Performance comparison between QD lasers grown on Si and on GaAs substrate. (1.3 µm InAs/GaAs QD active layer with ground-state lasing)

Reference			[27]	[4]	[28]	[29]	[30]	[31]	[32]
Substrate	Si	Si	GaAs	GaAs	GaAs	GaAs	GaAs	GaAs	GaAs
Threshold current [mA]	14.0	5.5	15.0	7.3	8.1	2.2	11.0	10.9	9.2
Dot density [× 10^{10} cm^{-2}]	4.9	4.9	3.0–4.0	5.0	4.0	5.9	6.0	6.6	N/A
Doping in active layer[cm^{-3}]	5 × 10^{17}	UID	UID	5 × 10^{17}	UID	*p*-doped	*p*-doped	*p*-doped	5 × 10^{17}
K-factor [ns]	0.92	1.3	2.4	0.82	1.7	0.74*	N/A	N/A	0.9
Measured f_{3dB} [GHz]	6.5	4.0	3.8	8.0	N/A	9.3	11.0	13.1	9.2
Modulation efficiency of f_r [GHz/mA$^{1/2}$]	0.68	1.11	N/A	0.93	0.5	N/A	1.22	N/A	0.92

*calculated from a given *K*-factor limited bandwidth
N/A stands for not available

The impedance of the QD laser was measured from reflection S_{11} characteristics to estimate the *RC* cutoff frequency. The measurement was performed using the LCA. The calibration was completed using an impedance standard substrate. The frequency dependence of impedance was measured for forward bias condition. The equivalent circuit model [33] used for a fitting is shown in Fig. 8(a). The model consists of an inductance *L*, a total capacitance *C* which includes a pad and junction capacitance, and a device resistance *R*. Z_0 and V_s stand for a characteristic impedance (50 ohm) and a voltage source, respectively. Although the S_{11} measurement was performed from 0.14 to 20 GHz, the circuit parameters were extracted by fitting the measured impedance up to 5 GHz because the measured S_{11} deviates from the S_{11} of circuit model at high frequencies. This would be caused by the wave-nature of the input RF signal propagating on the 580-µm-long stripe electrodes. We believe that the use of a co-planar transmission line electrode will solve this problem. Figure 8(b) shows 50-ohm normalized Smith chart of S_{11} characteristics of the QD laser. The forward bias current I_b of 80 mA was applied to the laser. The total capacitance was extracted to be 3.5 pF. The *p*-probe metal pad overlapped on the highly doped *n*-GaAs and *n*-metal as shown in Fig. 2(c), which is the primary reason for this large capacitance. The pad capacitance is calculated to be 2.2 pF by approximating the *p*-probe pad area to 105-µm-wide and 580-µm-long over a 1-µm-thick SiO_2 layer (RF dielectric constant $\varepsilon = 3.9$). The inductance *L* was negligibly small because the electrical contact was performed by a RF probe without any wire bonding. The *RC* cutoff frequency is calculated to be 7.7 GHz using the obtained circuit parameters ($C = 3.5$ pF, $R = 5.9$ Ohm). The pad capacitance can be reduced by depositing the metals on a thick dielectric and using the dielectric embedded channel ridge structure. Also, etching away highly doped *n*-GaAs buffer layer underneath *p*-probe metal will result in significant reduction of parasitic capacitance.

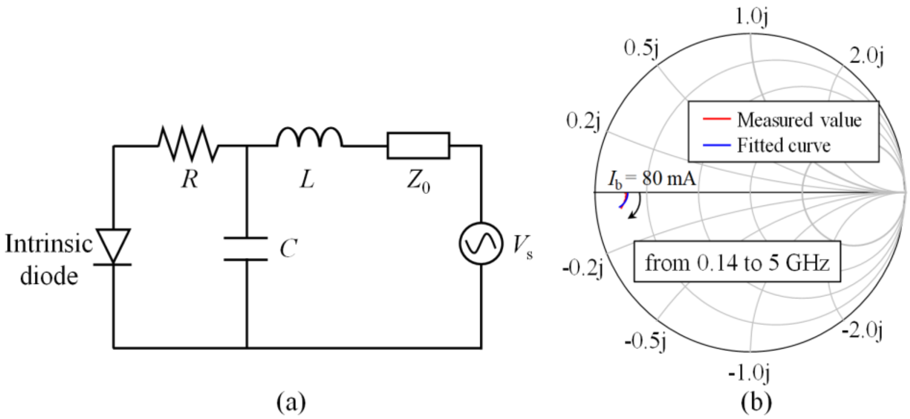

Fig. 8. Impedance measurement of QD laser on Si. (a) Equivalent circuit model used for the fitting. (b) Measured and fitted curves of reflection S_{11} characteristics for forward (80 mA) biased condition from 0.14 to 5 GHz.

4. Eye diagrams and bit-error-rate characteristics

A large-signal direct modulation for eye diagram and BER measurement was performed in back-to-back configuration at RT. The measured device is the same as shown in Fig. 4. A modulation signal and a bias current were applied to the QD laser by using the SG probe without 50 Ohm impedance matching. The modulation signal generated by a pulse pattern generator and DC bias current were combined by a bias-T. The optical power collected by a spherical-lensed fiber was divided by a 50:50 coupler. One of the divided optical power was connected to an optical power monitor. A variable optical attenuator was used to adjust the input power to a photoreceiver. Eye diagrams were captured by a sampling oscilloscope (Agilent 86100C equipped with HP83485A) without any low-pass filter. The modulation data-signal was non-return-to-zero (NRZ) with a pseudo-random bit sequence (PRBS) having a word length of 2^{31}-1. The modulation voltage swing was 2.0 V_{pp}. The bias current of the laser was fixed at 100 mA. Figure 9 shows eye diagrams measured at 7.5, 10, and 12.5 Gbit/s.

The suppressed overshooting due to the relaxation oscillation frequency was achieved thanks to the strong damping of the QD active layer. Eye openings were obtained with dynamic extinction ratios of 3.9dB, 3.7dB, and 3.3dB for each data-rate. To evaluate the obtained eye shape, an Ethernet mask test was performed for a 10.3125 Gbit/s eye diagram. Figure 10 shows the result of mask test using the 10 Gigabit Ethernet mask. No-violation to the mask was detected for measurement of 2027 waveforms. The measurement was stopped at this number of waveforms for the reason of the fluctuation of the alignment between the fiber and the QD laser which will affect the received power for long-time measurement. This result indicates an important step toward a practical application of QD lasers epitaxially grown on Si substrate. Appropriate low-pass filter as well as packaging for robust fiber alignment will provide further improvement in the eye diagrams.

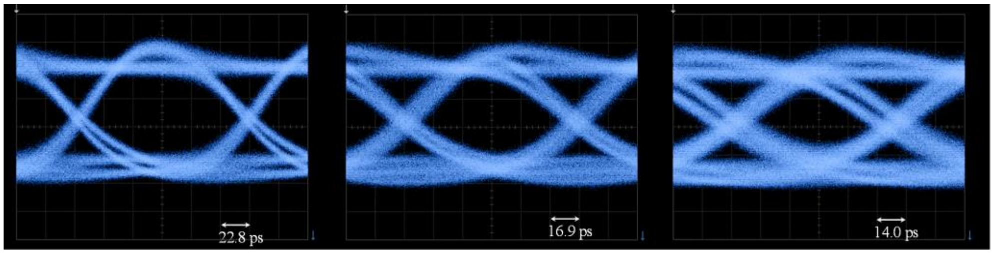

7.5 Gbit/s
Extinction ratio = 3.9dB

10 Gbit/s
Extinction ratio = 3.7dB

12.5 Gbit/s
Extinction ratio = 3.3dB

Fig. 9. Eye diagrams measured at 7.5, 10 and 12.5 Gbit/s using NRZ signal with PRBS of 2^{31}-1 patterns. The modulation voltage swing was 2.0 V_{pp}. The bias current of the QD laser was 100 mA.

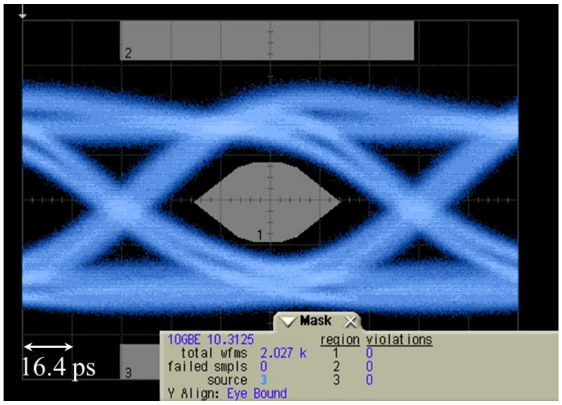

```
10GBE 10.3125          region violations
  total wfms  2.027 k     1       0
failed smpls  0           2       0
      source  3           3       0
Y Align: Eye Bound
```

Fig. 10. 10 Gigabit Ethernet mask test with 2027 waveforms.

BER characteristics in back-to-back transmission configuration were measured. The optical signal was detected and converted to an electrical signal by 10 GHz-band photoreceiver consisting of a *p-i-n* photodiode and a transimpedance amplifier (DSC-R402, Discovery Semiconductor, Inc.). The sensitivity of the photoreceiver for BER of 1 × 10^{-9} is −20 dBm for 10 Gbit/s. The modulation signal and the bias current conditions are same as the eye diagram measurement. Figure 11 shows BER curves for the data-rate of 7.5, 10, and 12.5 Gbit/s. From the BER curves, the minimum average received powers required to achieve a BER of less than 1 × 10^{-9} were –12.5, –9.5, and –3.4 dBm for the data-rate of 7.5, 10, and 12.5 Gbit/s, respectively. The PRBS pattern length dependence of BER was not observed. An error-floor could not be observed down to the BER of 1 × 10^{-13}. However, there is considerable power penalty of 6.1 dBm between the 10 Gbit/s and 12.5 Gbit/s. This is attributed to the bandwidth limitation of the QD laser. The possible reason for the change in the BER slopes between 7.5 Gbit/s and 10 Gbit/s is noise contribution from the rising and falling waveforms. The further improvement of data-transmission can be expected by reducing the *RC* parasitics and impedance matching of the laser chip. The packaged QD laser module with impedance matching has exhibited better BER performance than the measuring by RF probe because of the suppression of the electrical reflection [32].

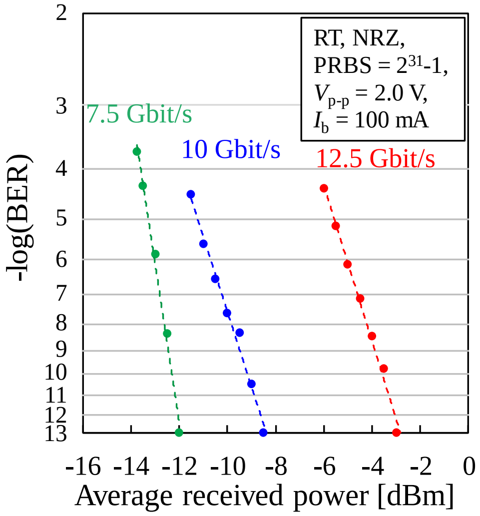

Fig. 11. BER versus average received power for 7.5, 10 and 12.5 Gbit/s.

We performed a 12 km transmission experiment on standard single-mode fiber (SSMF). The used fiber is 12-km-long (11559 m) Corning SMF-28 ULL fiber. The bias condition and the modulation signal were same as used in B2B configuration shown in Fig. 11. Fig. 12(a) shows 5 Gbit/s BER curves for B2B and after 10 km transmission. The inset figure shows static lasing spectrum at the bias current of 100 mA without modulation signal. The spectrum was centered at 1300 nm which was slightly deviated from the dispersion zero wavelength. Error free data-transmission was realized over 12 km. The minimum average received powers at BER of less than 1×10^{-9} were –12.6 and –11.6 dBm for the B2B and after 12 km. Thus, the power penalty through a 12 km SSMF was 1 dB. Figure 5(b) shows the eye diagrams of 5 Gbit/s signals for B2B and after 10 km transmission. Eye openings can be seen even after 10 km transmission while the waveform was affected by fiber dispersion. The extinction ratios were 3.9 dB and 3.8 dB for B2B and after 10 km, respectively. Regarding further improvement of transmission characteristics, a single-mode operation will enable QD lasers on Si to transmit over tens of km in a single-mode fiber. The performance result is mainly limited by the multimode lasing. We expect a low alpha-factor (the linewidth enhancement factor [34]) of ~0.5 or less, which is promising for efficient transmission [35]. Lastly, we also plan to study temperature-dependent direct modulation characteristics of our QD lasers on Si in future.

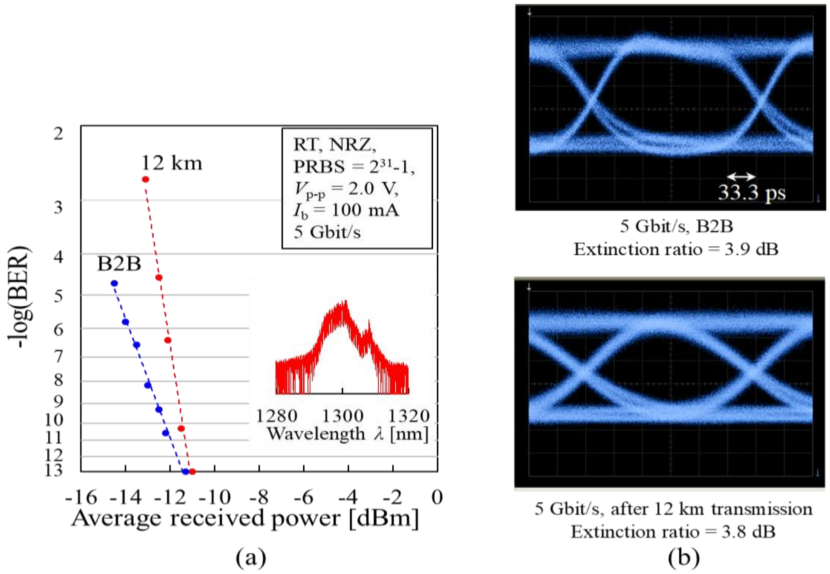

Fig. 12. 12 km SSMF transmission characteristics for 5 Gbit/s. (a) BER versus average received power. The inset shows static lasing spectrum at 100 mA. (b) Eye diagrams for B2B and after 12 km transmission.

5. Conclusion

In conclusion, we demonstrated direct-modulation of 1.3 µm QD laser grown on on-axis (001) Si substrate for the first time. The 580-µm-long QD laser with *p*-modulation doped active layer showed the 3dB bandwidth of 6.5 GHz at the bias current of 116 mA. The *p*-doped device has higher bandwidth than the unintentionally doped QD laser. The obtained *K*-factor of 0.92 ns indicates maximum *K*-factor limited $f_{3\text{dB, max}}$ of 9.5 GHz. Large signal modulation using NRZ signals confirmed open eyes at 12.5 Gbit/s. The 10 Gigabit Ethernet mask test resulted in no-violation for 2027 waveforms. The BER measurement in back-to-back configuration revealed no-error floor down to BER of 1×10^{-13} at the data-rate as high as 12.5 Gbit/s. 12 km SSMF transmission measurement revealed the power penalty of 1dB after transmission. Future work involves a dielectric embedded channel structure to reduce the capacitance and achieve a higher bandwidth and single-mode operation by adopting a DFB cavity. This work demonstrates the compatibility of QD laser grown on Si with low-cost and wafer scale fabrication of directly modulated light sources.

Funding

Advanced Research Projects Agency-Energy (ARPA-E) (DE-AR0000672); Japan Society for the Promotion of Science (JSPS) Grants-in-Aid for Scientific Research (KAKENHI) (15J11776).

Acknowledgments

The authors would like to thank Kurt Olsson, John English for their MBE assistance and Zeyu Zhang and Daniel Blumenthal for assistance.